Nonlinear Dyn (2008) 52: 347–359
DOI 10.1007/s11071-007-9283-5

ORIGINAL PAPER

Analysis for the optimal location of cable damping systems on stayed bridges

Roberto Alvarado Cárdenas · Francisco Javier Carrión Viramontes · Aurelio Domínguez González · Gilberto Herrera Ruiz

Received: 31 August 2006 / Accepted: 30 May 2007 / Published online: 4 August 2007

Abstract Computational models are increasingly being used for the dynamic analysis of structures with nonlinear or uncertain behavior, such as cables in stayed bridges, which nowadays are progressively more used as an alternative for long span and slim structures. In this work, a 3D nonlinear model is described to evaluate the wind dynamic effects on cables for this type of bridges under different scenarios, but also for health monitoring and structural simulation to guarantee performance, evaluate load capacity and estimate life prediction. Fatigue is one of the most relevant and complex failure causes in highway bridges, particularly on the anchorage elements of the cables in stayed bridges; where dampers may be used to minimize the dynamic behavior of the structure and reduce fatigue damage. With this nonlinear simulation model, different damper locations and configurations are evaluated to find the optimal position. A feasibility function is used as a weighting function to take into account the damper's size and design. Analysis is particularly focused for a real cable stayed bridge in the state of Veracruz in México.

R.A. Cárdenas (✉) · F.J.C. Viramontes · A.D. González · G.H. Ruiz
Universidad Autónoma de Querétaro, Cerro de las Campanas s/n Querétaro Qro., Mexico 76000, Mexico
e-mail: ralvarad@itesm.mx

F.J.C. Viramontes
Instituto Mexicano del Transporte, Sanfandila, Querétaro, Mexico

Although the geometry, the forces and the stresses on cable structures are a challenge, even for structural specialists, the results from this work using the proposed 3D nonlinear model showed to be accurate for the simulation of many different wind scenarios, and damper's location and orientations. Finally, the feasibility weighting function enabled the geometrical limitations to estimate the best location of a damper system to minimize the risk for fatigue failure.

Keywords Vibration control · Cable stayed bridge · Damping systems

1 Introduction

Since the second half of the last century to these days, the cable-stayed bridge concept has been widely used for long span bridges like the Millau Viaduct in France and many others built around the world. With these types of bridges, when the length of the span is increased, their behavior becomes more complex and structural characteristics such as stiffness, external forces and dynamic stability, are even more important to evaluate structural reliability and safety [1]. With large spans, the cable-stayed bridges are more sensitive to flutter instability, wind, earthquakes and traffic-induced vibrations, where highly nonlinear behavior and structural coupling between cables and bridge deck, are some of the specific and complex

problems to solve [2]. At the same time, many long bridges are located where adverse environment and strong winds are present; conditions that may cause large deflections and considerable vibrations on cable-stayed bridges by buffeting and self-excited forces [3], causing fatigue and structural deterioration.

The detailed structural dynamic analysis of the cable-stayed bridges is very important and in many cases, full behavior analysis is recommended under extreme shaking conditions to evaluate the wind's effect on the structure's dynamic behavior [4]. In general, appropriate simulation models for bridges are particularly important for dynamic analysis, to identify structural problems and to prevent disasters [5]. One of the most significant techniques used for bridge structural assessment is the Finite Element Method (FEM). In modern practice, Finite-Element (FE) models are effective for nonlinear analysis of suspended bridges, where geometric nonlinear theory can include the inherent effects in suspended bridges such as cable sags, large deflections, axial forces and the relations between the bending moments to the bridge stiffness. Two or three-dimensional models with beam and truss elements are often used for both the superstructure and the substructure of cable-supported bridge [6].

The dynamic analysis of a cable-stayed bridge under dynamic loads such as wind, earthquakes and traffic, is very complex and it requires considerable computational time [7]. Many studies evaluate the effect of the dynamic forces on bridges [8–13], the overall structural integrity [14–18] and the modal characteristics of the structures [19–23]; however, few works related to the cables or to the cable-bridge connecting elements have been published. In general, more research is required to analyze specific problems on the cables and connecting elements due fatigue damage, and to development intelligent damping systems to reduce the dynamic fatigue effects [24–26].

In this paper, a detailed simulation study of the Río Papaloapan cable-stayed bridge (located in México) is presented. The wind dynamic forces on the cables were analyzed, and a sensibility evaluation was completed to define the best damping system configuration. The 3D simulation model of the bridge cables is based on the nonlinear theory which has being modified to include different damping configurations to find the most favorable condition.

2 Nonlinear cable model

In order to find the best location for a cable vibration control system in a cable stayed-bridge, a simulation 3D model was developed by Carrion [27] based on the nonlinear formulation presented by Xu et al. [28], to perform the dynamic behavior of the cable under different load and wind conditions.

Our studied case is based on the Río Papaloapan Bridge (Fig. 1), located in the state of Veracruz in México. The total length of the bridge is 342.7 m,

Fig. 1 Papaloapan bridge picture

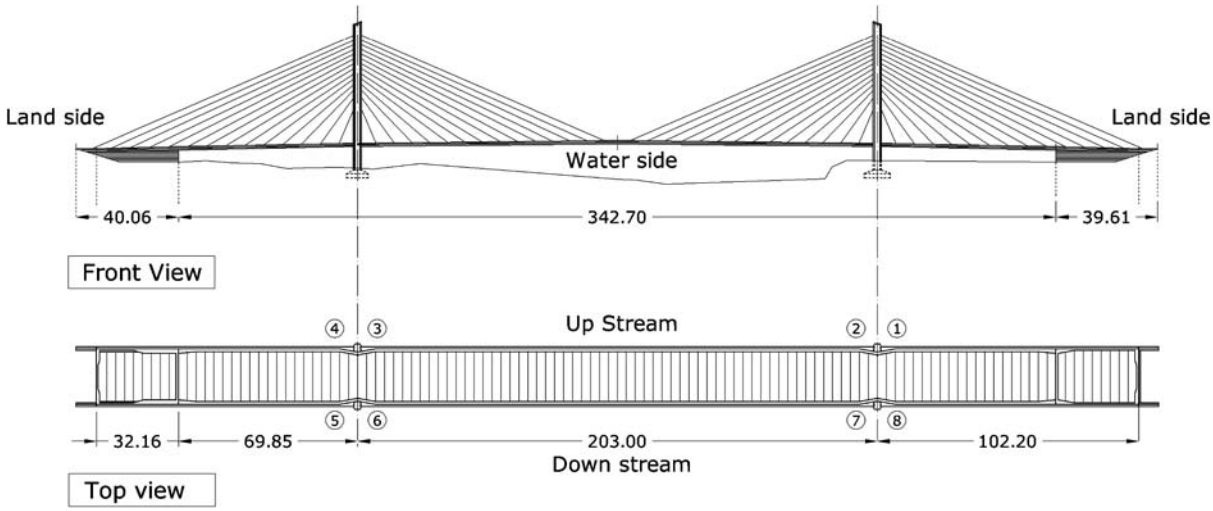

Fig. 2 Front and top view drawings of the bridge

with two towers and eight semi-harps with 14 cables each one (Fig. 2). The location of the bridge is near the Cosamaloapan de Carpio City and the cable-stayed bridge is over the Papaloapan River that is one of the most important rivers in México.

The city of Veracruz, which is the capital of the state with the same name, is the most important marine port in México. The relevance of the Río Papaloapan Bridge, located at 45 km from the coast, is that it communicates this port with the southern oil fields. Another remarkable aspect of the state of Veracruz is that it has a long coastline with the Gulf of México, widely known for its hurricanes and gusty winds. Clearly, the importance of the dynamic analysis and structural evaluation of this bridge is evident, in order to minimize the risk of failure of any of its structural components, particularly the cables.

As it was mentioned, the wind effect is one of the most important hazards on the bridge, and to evaluate the wind effect on the cable stayed bridge, a computer model was developed based on the following: the catenary's profile of the cable in the static state is calculated from the traditional equation [29]

$$y = \frac{H}{mg}\left\{\cosh\left(\frac{mgl}{2H}\right) - \cosh\frac{mg}{H}\left(\frac{l}{2} - x\right)\right\} \tag{1}$$

where y is the vertical component of the cable shape, x is the horizontal component, m is the mass of the cable, g is the gravitational force, l is the initial length of the cable, and H is the horizontal component of the tension on the cable. Figure 3 shows a diagram of the reference coordinates, the external loads and displacements of the cable.

The next equations are used to relate the coordinate dimensions to the tension components on the cable [29].

$$L = \frac{HL_0}{EA_0} + \frac{HL_0}{W}\left\{\sinh^{-1}\left(\frac{V}{H}\right) - \sinh^{-1}\left(\frac{V-W}{H}\right)\right\}, \tag{2}$$

$$R = \frac{WL_0}{EA_0}\left(\frac{V}{W} - \frac{1}{2}\right) + \frac{HL_0}{W}\left[\left\{1 + \left(\frac{V}{H}\right)^2\right\}^{1/2} - \left\{1 + \left(\frac{V-W}{H}\right)^2\right\}^{1/2}\right] \tag{3}$$

here, E is the elasticity module of the cable material, A_0 is the transverse section area, W is the weight, L_0 is the initial length and H and V are the horizontal and vertical tension components on the cable, L represents the horizontal distance between the ending points of the cable and R the vertical distance. Once these last two parameters are given, a numeric algorithm, like Newton–Raphson optimization method, is required calculate the cable tension components.

This nonlinear model is useful for big deformations on cables or to calculate variations on tension values. In the case of the cable-stayed bridge, it is applied to evaluate the cable's performance under fluctuating

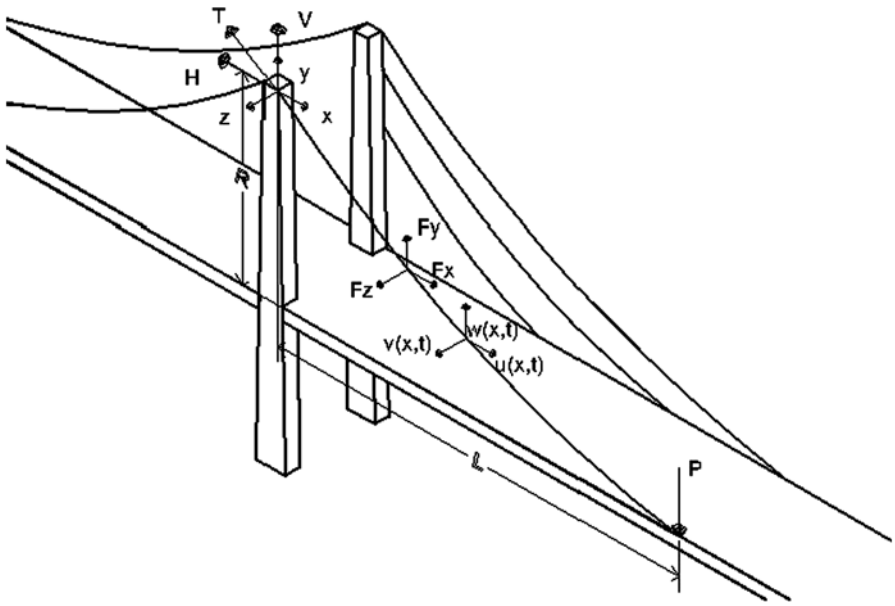

Fig. 3 Cable diagram

dynamic forces from earthquake, wind or traffic. In Fig. 3, the geometry, dimensions, and variables of the model are shown.

The components of the displacements are related with the forces by the next equations

$$\frac{1}{\sqrt{1+(\frac{dy}{dx})^2+(\frac{dz}{dx})^2}}\frac{\partial}{\partial x}\left(H\frac{\partial u}{\partial x}+h\right)+F_x(x,t) = m\frac{\partial^2 u}{\partial t^2}+c\frac{\partial u}{\partial t}, \tag{4}$$

$$\frac{1}{\sqrt{1+(\frac{dy}{dx})^2+(\frac{dz}{dx})^2}}\frac{\partial}{\partial x}\left(H\frac{\partial w}{\partial x}+\frac{\partial y}{\partial x}h\right)+F_y(x,t) = m\frac{\partial^2 w}{\partial t^2}+c\frac{\partial w}{\partial t}, \tag{5}$$

$$\frac{1}{\sqrt{1+(\frac{dy}{dx})^2+(\frac{dz}{dx})^2}}\frac{\partial}{\partial x}\left(H\frac{\partial v}{\partial x}+\frac{\partial z}{\partial x}h\right)+F_z(x,t) = m\frac{\partial^2 v}{\partial t^2}+c\frac{\partial v}{\partial t} \tag{6}$$

where u, w and v represent the displacements of the cable with respect to the static initial position, under the effect of the F_x, F_y and F_z external forces, h is the internal tension of the cable and it is calculated from the following equation:

$$h = \frac{EA_0}{(1+(\frac{dy}{dx})^2+(\frac{dz}{dx})^2)^{3/2}} \times\left[\frac{du}{dx}+\frac{dy}{dx}\frac{dw}{dx}+\frac{dz}{dx}\frac{dv}{dx}\right]. \tag{7}$$

Initially, $\frac{dy}{dx}$ and $\frac{dz}{dx}$ are calculated from the equilibrium equations, so that $\frac{dz}{dx}=0$ and the nonlinear parameter $\frac{dy}{dx}$ is obtained in the following section.

2.1 Evaluation of the nonlinear parameter

In order to get the $\frac{dy}{dx}$ value, it is necessary to start from the static solution of a tensioned cable and to use the Lagrangian coordinates of the deformed cable, the following relation is obtained as follows:

$$\left(\frac{dx}{dp}\right)^2+\left(\frac{dy}{dp}\right)^2=1 \tag{8}$$

where x and y are the Cartesian coordinates, p and s are the Lagrange coordinates of the deformed and unreformed cable, respectively. From the forces balance it is obtained:

$$\frac{dx}{dp}=\frac{H}{T}, \tag{9}$$

$$\frac{dy}{dp}=\frac{V}{T}-\frac{W}{T}\frac{s}{L_0}. \tag{10}$$

In this case, L_0 is the undeformed length of the cable and its total weight is $W=mgL_0$, where m is the mass

per unit length. By substituting (9) and (10) on (8), it is obtained

$$\frac{H^2}{T^2}+\frac{V^2}{T^2}+\frac{W^2}{T^2}\frac{s^2}{L_0^2}-\frac{2VWs}{T^2L_0}=1. \tag{11}$$

Where the tension force is obtained as a function of s like

$$T=\left\{H^2+\left(V-\frac{Ws}{L_0}\right)^2\right\}^{1/2}. \tag{12}$$

On the other side, it is obtained that

$$T=EA_0\left(\frac{dp}{ds}-1\right). \tag{13}$$

As a result,

$$\frac{dx}{ds}=\frac{dx}{dp}\frac{dp}{ds}=\frac{H}{T}\left(\frac{T}{EA_0}+1\right)$$
$$=\frac{H}{EA_0}+\frac{H}{T}=\frac{H}{EA_0}+\frac{H}{[H^2+(V-\frac{Ws}{L_0})^2]^{1/2}}, \tag{14}$$

$$\frac{dy}{ds}=\frac{dy}{dp}\frac{dp}{ds}=\left(\frac{V}{T}-\frac{W}{T}\frac{s}{L_0}\right)\left(\frac{T}{EA_0}+1\right)$$
$$=\left(V-\frac{Ws}{L_0}\right)\left\{\frac{[H^2+(V-\frac{Ws}{L_0})^2]^{1/2}+EA_0}{EA_0[H^2+(V-\frac{Ws}{L_0})^2]^{1/2}}\right\}. \tag{15}$$

Finally, from (14) and (15), it is obtained that:

$$\frac{dy}{dx}=\frac{V}{H}-\frac{W}{H}\frac{s}{L_0}. \tag{16}$$

To obtain $\frac{dy}{dx}$, the static equations obtained by Irving [25] are used:

$$x(s)=\frac{Hs}{EA_0}+\frac{HL_0}{W}\left[\sinh^{-1}\left(\frac{V}{H}\right)\right.$$
$$\left.-\sinh^{-1}\left(\frac{V-\frac{Ws}{L_0}}{H}\right)\right], \tag{17}$$

$$y(s)=\frac{Ws}{EA_0}\left(\frac{V}{W}-\frac{s}{2L_0}\right)+\frac{HL_0}{W}\left\{\left[1+\left(\frac{V}{H}\right)^2\right]^{1/2}\right.$$
$$\left.-\left[1+\left(\frac{V-\frac{Ws}{L_0}}{H}\right)^2\right]^{1/2}\right\}. \tag{18}$$

Finally, by obtaining the derivative of (17) and (18), we got:

$$\frac{dy}{dx}=\frac{\frac{dy}{ds}}{\frac{dx}{ds}}. \tag{19}$$

2.2 Determination of the h function

For the calculation of the h function on (4) and (5), it is made the balance forces according with the Fig. 4.

From the geometric analysis it is obtained that:

$$ds^2=dx^2+dy^2, \tag{20}$$

$$ds'^2=(dx+du)^2+(dy+dw)^2. \tag{21}$$

The next equation can be deduced from (20) and (21)

$$\frac{ds'-ds}{ds}=\sqrt{\frac{(dx+du)^2+(dy+dw)^2}{dx^2+dy^2}}-1. \tag{22}$$

Replacing and taking a first order approximation from the Taylor expansion:

$$\frac{ds'-ds}{ds}=\frac{dx}{ds}\frac{du}{ds}+\frac{dy}{ds}\frac{dw}{ds}. \tag{23}$$

On the other side, the dynamic tension T_d respect to h is

$$T_d=h\frac{ds}{dx} \tag{24}$$

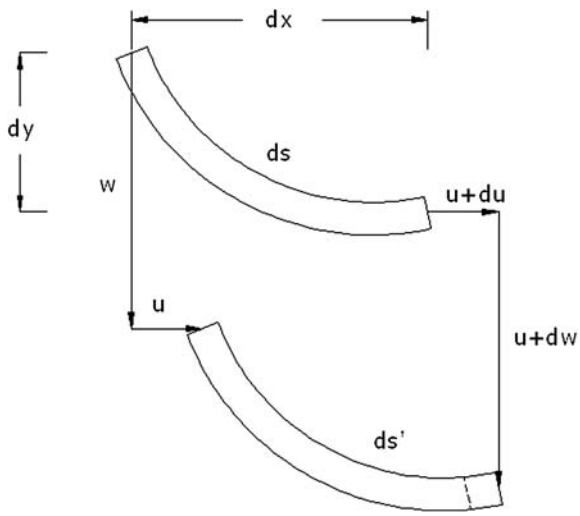

Fig. 4 Deformation diagram for a cable section

by the Hook's Law, we have

$$\frac{ds' - ds}{ds} = \frac{T_d}{EA_0} = \frac{h}{EA_0}\frac{ds}{dx}. \tag{25}$$

So that it is obtained the equation that describes the h function

$$h = \frac{EA_0}{(\frac{ds}{dx})^3}\left(\frac{du}{dx} + \frac{dy}{dx}\frac{dw}{dx}\right) \tag{26}$$

and

$$\frac{ds}{dx} = \sqrt{1 + \left(\frac{dy}{dx}\right)^2} \tag{27}$$

then, the final 2D representation for the h function is:

$$h = \frac{EA_0}{(1 + (\frac{dy}{dx})^2)^{3/2}}\left[\frac{du}{dx} + \frac{dy}{dx}\frac{dw}{dx}\right]. \tag{28}$$

By a similar procedure the 3-D equation for the h function is obtained

$$h = \frac{EA_0}{(1 + (\frac{dy}{dx})^2 + (\frac{dz}{dx})^2)^{3/2}} \times \left[\frac{du}{dx} + \frac{dy}{dx}\frac{dw}{dx} + \frac{dz}{dx}\frac{dv}{dx}\right]. \tag{29}$$

3 Numerical solution scheme

The numerical model was programmed in Fortran 90 and the results of the simulation were analyzed using the MatLab software to handle the graphic results. Figure 5 shows the flow chart of the numerical solution scheme of the model.

The solution process in the model begins with the static solution to obtain the initial conditions of the cable geometry. In order to evaluate the dynamic behavior of the cable, the Runge–Kuta 4 integration method is used for the best approximation and numerical stability of the model because of its intrinsic characteristics. The discreet model was obtained using Finite Differences (FD) and the precision of the model was evaluated comparing the vector norms between many different discreet method choices. For the analysis of the cable dynamics, the difference of the norms was set to be less than 0.5%. The model calibration was resulted from experimental field vibrations measurements.

The convergence analysis of the model was evaluated by reducing the time step until no difference was found within a 0.1% among the obtained results.

4 Wind model approximation

The wind effect on the cables of the bridge is calculated from the traditional drag equation from fluid dynamics theory of immersed bodies [30], that is:

$$f = CA\rho\frac{U^2}{2}. \tag{30}$$

On this equation, f is the drag force of the wind, C is the shape coefficient, A is the section area and U is de wind speed.

Statistical analysis of the wind velocity measurements from three meteorological stations located around the bridge area provided the wind load information necessary for the Río Papaloapan Bridge model. Figure 6 shows a typical sample of the wind speed behavior.

5 Model calibration

To calibrate the cable's model, field data measured in 2003 during an experimental study to evaluate the structural integrity of the bridge, was used. In this case, a low frequency accelerometer (TEC 195) and a portable data logger and analyzer (TEC SmarMeter 1330 ULF) were used, and the accelerometer was located perpendicular to the cable at 2 meters height from the bridge's deck (Fig. 7). Four independent measurements during 16 seconds at 60 Hz sampling rate were recorded using soft wind ambient excitation, and the natural vibration modes were identified from the frequency response functions (Fig. 8). Table 1, shows the frequency for the first three modes of cable 12 in semi-harp 7, where no variation on the frequency is observed for the different tests and to the equipment's accuracy and test conditions; these results show that the experiment was controlled up to a certain level despite to the ambient excitation. Also, it should be mentioned that the fist vibration frequency was not always identified due to the accelerometer location, and the cable behavior is linear.

Cable's damping coefficient was calculated using the resonant amplification method [31], and the final value used for the model resulted from the average of the identified frequency peaks of the first three

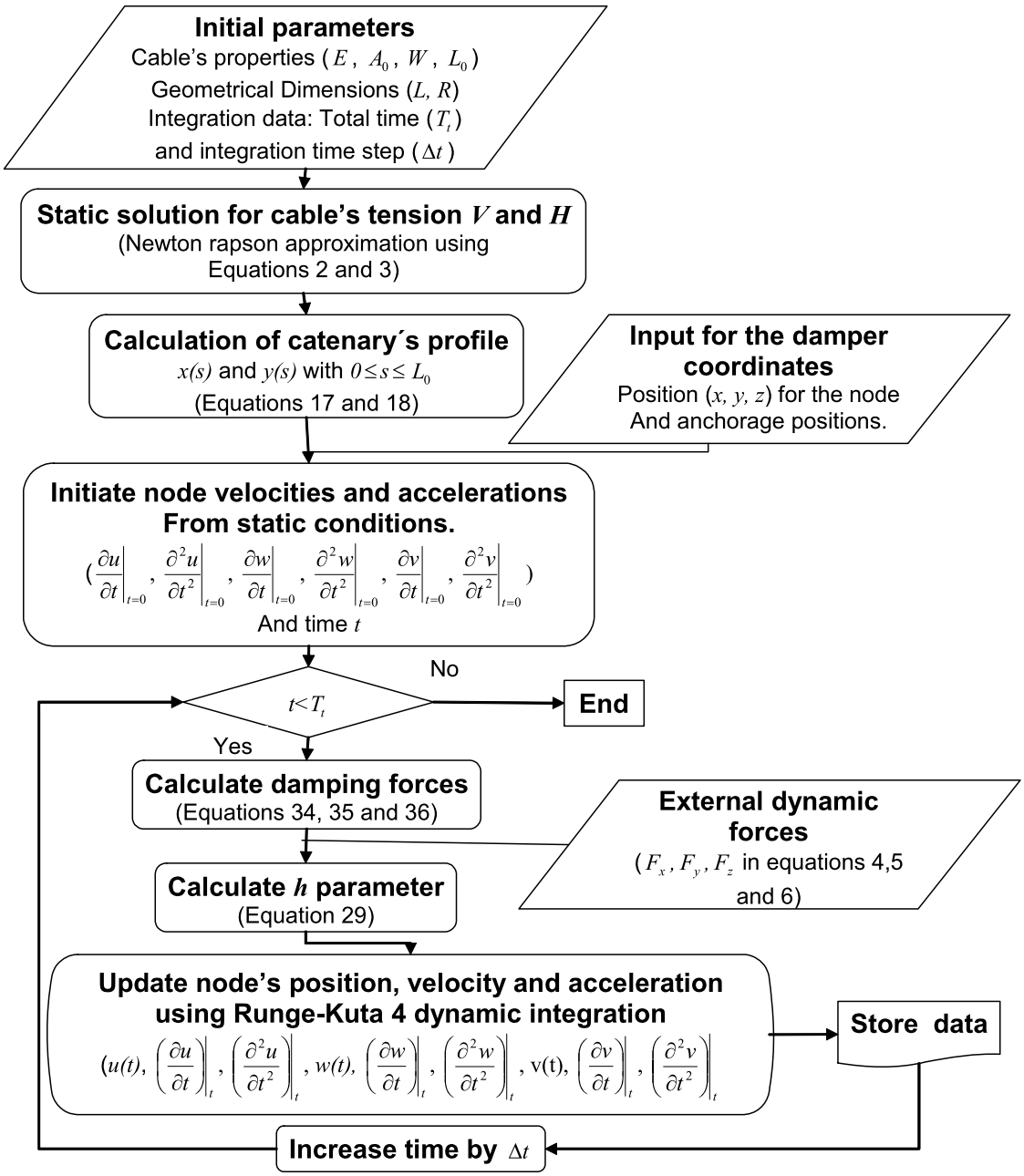

Fig. 5 Solution scheme flow chart

vibration modes. In this case, the damping ratio was 0.078 ± 0.007, equivalent to a damping coefficient of 7.8 kg/s per node [32], assuming all constant for all nodes.

Final calibration of the model was achieved by changing the mass per unit length of the cable, until the model's modal frequencies matched the experimental values.

To evaluate the discretization dependency, starting from 25, the number of segments in the numerical model was duplicated until dynamic responses from consecutive divisions were similar within an ac-

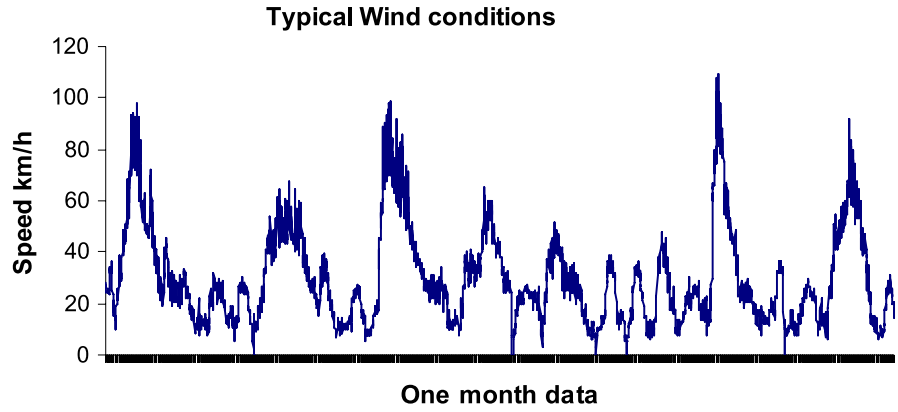

Fig. 6 Typical wind conditions on the bridge

Fig. 7 Vibration experimental setup

ceptable percentage. Results were compared using the Euler norm of the time responses until a 0.1% difference was obtained. Table 3 presents the evaluation from 101 to 201 nodes and from 201 to 401 nodes, for locations at ¼, ½ and ¾ of the total length of the cable. Since little difference was found from 101 segments or more, this value was chosen for the final calibrated model.

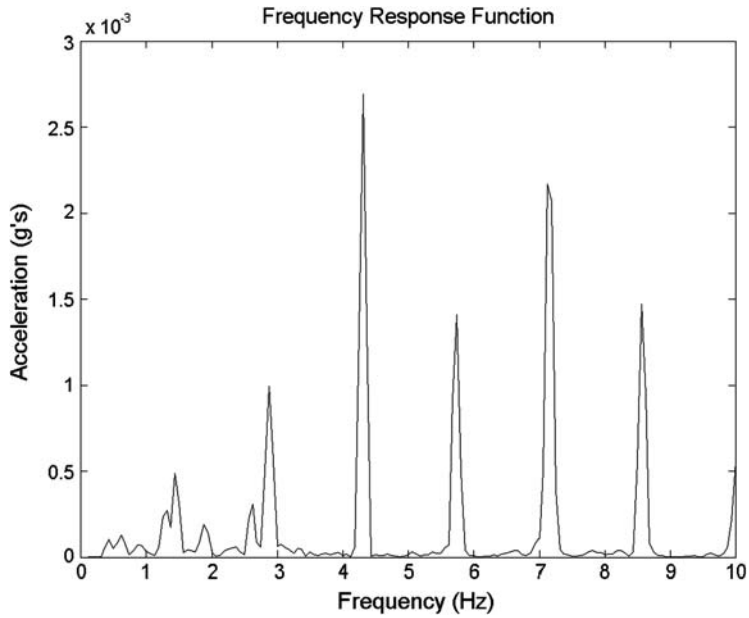

Fig. 8 Frequency response function

Table 1 Frequency for the first three modes of cable

	1st mode	2nd mode	3rd mode
Test 1	1.4375	2.875	4.313
Test 2	1.4375	2.875	4.313
Test 3	N/A	2.875	4.313
Test 4	N/A	2.875	4.313
Average	1.4375	2.875	4.313

6 Practical application on a cable stayed bridge

In order to evaluate the effect of the damping system on the cable model, the damper acting forces were simulated in the nonlinear system, (see (4), (5) and (6)), resulting as follows:

$$\frac{1}{\sqrt{1+(\frac{dy}{dx})^2+(\frac{dz}{dx})^2}}\frac{\partial}{\partial x}\left(H\frac{\partial u}{\partial x}+h\right)$$
$$+R_x(t)+F_x(x,t)=m\frac{\partial^2 u}{\partial t^2}+c\frac{\partial u}{\partial t}, \quad (31)$$

$$\frac{1}{\sqrt{1+(\frac{dy}{dx})^2+(\frac{dz}{dx})^2}}\frac{\partial}{\partial x}\left(H\frac{\partial w}{\partial x}+\frac{\partial y}{\partial x}h\right)$$
$$+R_y(t)+F_y(x,t)=m\frac{\partial^2 w}{\partial t^2}+c\frac{\partial w}{\partial t}, \quad (32)$$

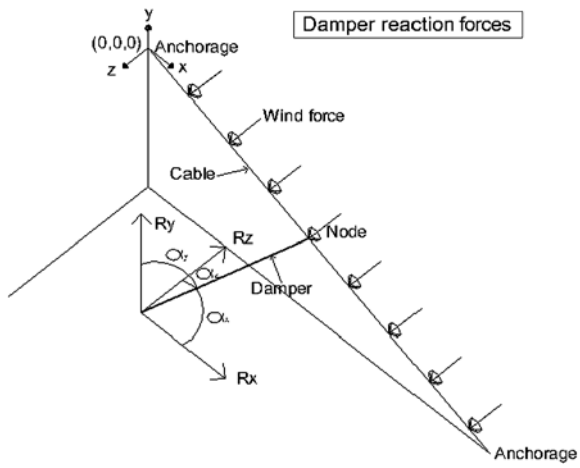

Fig. 9 Damper reaction forces

$$\frac{1}{\sqrt{1+(\frac{dy}{dx})^2+(\frac{dz}{dx})^2}}\frac{\partial}{\partial x}\left(H\frac{\partial v}{\partial x}+\frac{\partial z}{\partial x}h\right)$$
$$+R_z(t)+F_z(x,t)=m\frac{\partial^2 v}{\partial t^2}+c\frac{\partial v}{\partial t}. \quad (33)$$

In these equations, R_x, R_y and R_z are the damping reacting forces in the tree dimensional directions as shown in Fig. 9.

The damper force is defined in terms of the directional cosine of their displacement and velocity vec-

tors:

$$R_x(t) = K u \,\mathrm{Cos}(\alpha_x) + c\left(\frac{\partial u}{\partial x}\right)\mathrm{Cos}(\alpha_x), \tag{34}$$

$$R_y(t) = K w \,\mathrm{Cos}(\alpha_y) + c\left(\frac{\partial w}{\partial y}\right)\mathrm{Cos}(\alpha_y), \tag{35}$$

$$R_z(t) = K v \,\mathrm{Cos}(\alpha_z) + c\left(\frac{\partial v}{\partial z}\right)\mathrm{Cos}(\alpha_z). \tag{36}$$

In the previous equations, K is the stiffness of the damper, c is the damping coefficient of the damper and de $\alpha_x, \alpha_y, \alpha_z$ are the angles with respect to the x, y and z coordinates, respectively.

To analyze the best location for the damping system, the geometrical and material parameters of the cables from the Río Papaloapan Bridge are presented in Table 2.

Table 2 Initial calibrated parameters

Variable	Units	Value
Elasticity Module (E)	kg/cm^2	2 010 000
Travers section Area (A_0)	cm^2	40.4115
Mass per length unit (m)	kg	36.7584
Vertical distance (R)	m	39.25
Horizontal distance (L)	m	85.13
Initial length of the cable (L_0)	m	93.4175
Damping coefficient of the cable (c)		7.8
Static Vertical force (V)	kg	118 014
Static Horizontal force (H)	kg	252 230
Damper strain (K_a)		1
Damping coefficient of the damper (C_a)		2, 20

Previous to the analysis, the most significant parameters related to the wind dynamic loads were evaluated, such as frequency, magnitude, time-frequency behavior, direction, and maximum and minimum values. From this examination, the most representative wind load conditions were defined to simulate the wind drag force on the bridge's cables. The following table shows the different scenarios for the wind loads.

By simulating different wind scenarios, it was found that the cable's displacements are more significant when the wind direction is perpendicular to the semi-harp plane of the bridge (x–y plane). This condition was defined as the most critical condition.

To evaluate the damper's effect on the dynamic behavior of the cable, different geometrical configurations for the damper were studied by changing the location of its fixing endpoint to the deck. The reference location was taken when the damper's orientation was perpendicular to the x–z plane; that is, when the damper is aligned parallel to the y direction.

To define the geometrical configuration of the damper, three different variables are associated to the fixing endpoints (the one to the deck and the other to the cable); the node identification number on the cable (for the upper endpoint) and the (x, z) coordinates with respect to the reference location for the lower endpoint. In addition to the reference location, eight locations were defined in the x–z plane as it is illustrated in Fig. 10. Additionally, to evaluate the damper's performance for different angle orientations, an additional location (number 9) was placed on the y–z plane at half distance of the z coordinate of point 7 (Fig. 10).

Since the cable was divided into 100 segments, that is, 101 nodes; to simplify the analysis, the upper fixing endpoint of the damper was located at every 10 nodes,

Table 3 Cable segments

Number of nodes		Norm difference (%)		
1st choice	2nd choice	¼ cable length	½ cable length	¾ cable length
101	201	0.0999	0.0995	0.1011
201	401	0.0250	0.0249	0.0253

Table 4 Input external forces

Charge type	Application time	Vector components of the force	Dynamic of the force
Punctual	Instantaneity	Magnitude	Fix
Distributed	Constant	Direction	Variable
Growing	Fluctuant	Way	

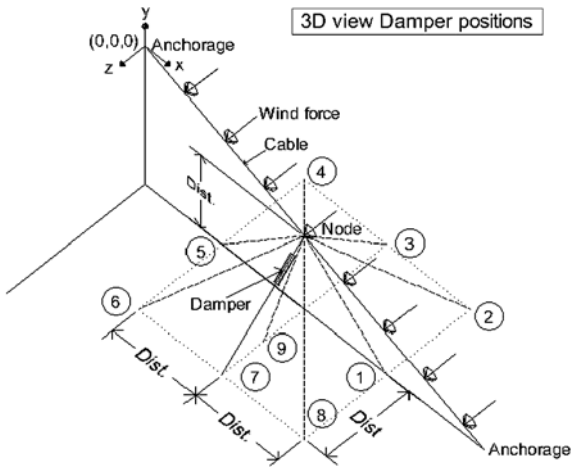

Fig. 10 3D view damper positions

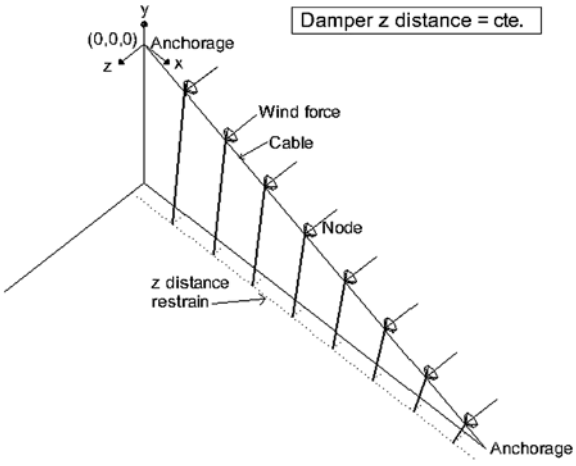

Fig. 11 Damper z distance to semi-harp plane

that is, 9 node locations were simulated along the cable; that is, 81 different conditions to be simulated.

Finally, considering the geometrical characteristics and limitations of the bridge, the lower fixing endpoint of the damping system was restricted up to 3 meters distance from the reference location for the z coordinates (Fig. 11).

7 Results

Results from the analysis to find the best location for the damping system are shown in Fig. 12.

It can be seen in Fig. 12 that the best location for the damper is almost at the middle of the cable (Node 40), oriented against the wind force and with the lowest possible acute angle. As it was mentioned previously, the geometry of the traverse section of the bridge deck, limits the fixing endpoint position of the damper, thus, a limited number of scenarios for the cable damper configuration were analyzed where this fixing endpoint was located to a distance within 3 meters from the semi-harp plane (Fig. 13).

In Fig. 13, the best point for the damper system is at the center of the cable, which is not a realistic location that would require a very large and sophisticated system. A more rational analysis to locate the damper requires the consideration of certain strategies to take into account the size and geometrical characteristics of the system and to define a more plausible location.

Finally, for a realistic analysis, a feasibility weighting function is defined to take into account the size and the possible locations for the damper. In this case, results show a strong dependence to the weighting function and that, for the entire configuration cases considered for this study, the best design choices for the damper are those with the lowest possible acute angle that induces the biggest reaction force against the wind drag force. Results in Fig. 14, show that a possible location for the damper is within nodes 95 to 98.

8 Conclusions

The extreme wind forces acting on the Papaloapan Bridge call for the application of the nonlinear model described in this work, despite the fact that the cable of the bridge is subject to a high tension force. In our study case, the cable system is more sensitive to external forces applied on z direction, because the tension in the cable has components on x and y that minimize the displacement of the nodes on those directions, so that the reaction forces of the damping system have better response when it is oriented against the wind direction.

In the first part of the analysis, it was found that the most favorable location for the damper system was within the center of the cable, where the largest displacements take place. The previous analysis was done assuming none geometrical restrictions for the damper system; nonetheless, for real implementation some restrictions exist, such as the damper's size or the lower fixing endpoints location with respect to the semi-harp plane.

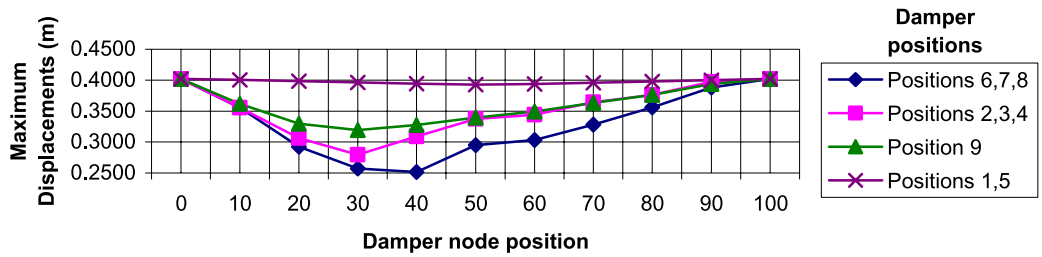

Fig. 12 Damper maximum displacements for all nodes and damper position

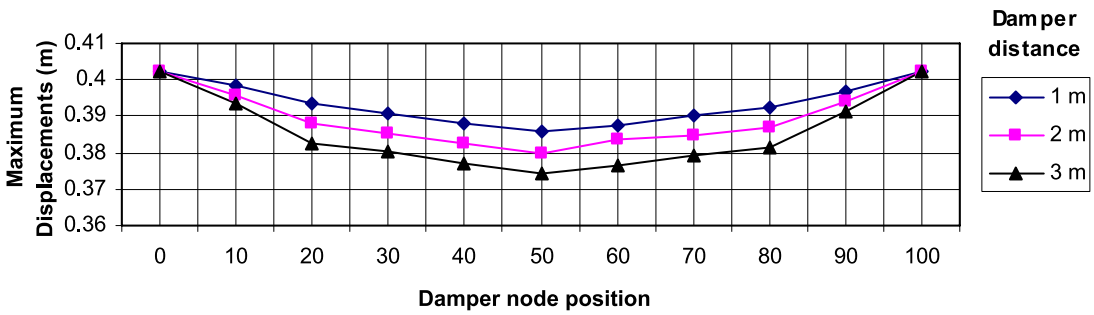

Fig. 13 Cable maximum displacements to damper node position and distance to semi-harp plane

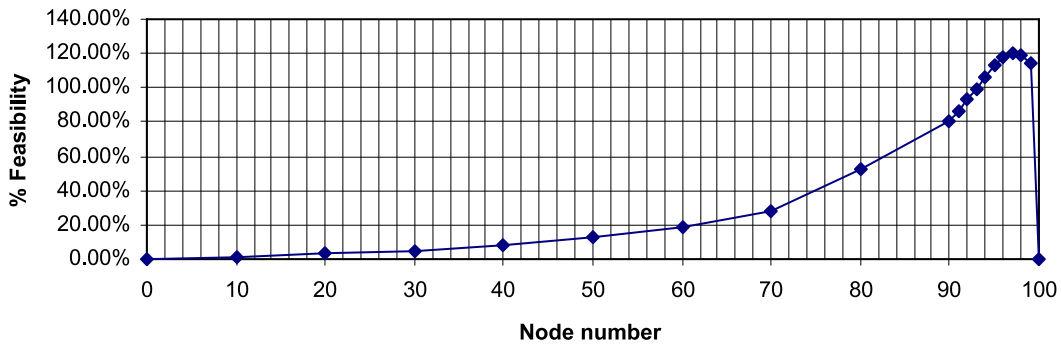

Fig. 14 Damper feasibility analyses

When the bridge geometry and damper size restrict the damper fixing endpoint position, the central node is no more the best location. In such cases, an appropriate analysis must include a feasibility weighting function to consider restriction such as the damper orientation, the damper size, the cost, the esthetics of the bridge, and the undesirable intrinsic dynamic properties that the damper may produce on the bridge.

The 3D nonlinear model showed to be adequate for the analysis of different scenarios and dynamic structural problems, particularly to the analysis of the bridge under the effect of external wind drag force. With this methodology, and a complete structural model of the bridge (including the deck, piles), it is also possible to estimate the behavior of the bridge structure under different dynamic forces like earthquakes or traffic conditions.

Acknowledgements The authors want to thank Dr. Aaron Sariñana Toledo, from the Instituto Tecnológico y de Estudios Superiores de Monterrey, Campus Querétaro for his assistance, to the Servicio Meteorológico National and to the Departamento hidro meteorológico of the Comisión Federal de Electricidad for the meteorological information of the studied bridge.

References

1. Fag, I., Chen, Ch., Chang, I.: Field static load test on Kao–Ping–Hsi cable-stayed bridge. J. Bridg. Eng. **9**(6), 531–540 (2004)
2. Xu, Y., Xia, H., Yan, Q.: Dynamic response of suspension bridge to high wind and running train. J. Bridg. Eng. **8**(1), 46–55 (2003)
3. Zhu, L., Xu, Y., Zhang, F., Xing, H.: Buffeting of a long Suspension Bridge: Analysis and field measurement. In: Health Monitoring and Management of Civil Infrastructure Systems. Proceedings of the SPIE, vol. 4337, pp. 323–334 (2001)
4. Achire, Y., Bossens, F., Preumont, A.: Active damping and flutter control of cable-stayed bridge. J. Wind Eng. Ind. Aerod. **74–76**, 913–921 (1998)
5. Xia, P., Brownjohn, J.: Bridge Structural condition assessment using systematically validated finite-element model. J. Bridg. Eng. **9**(5), 418–423 (2004)
6. Ren, W., Blandford, G., Harik, I.: Roebling suspension bridge, I: finite-element model and free vibration response. J. Bridg. Eng. **9**(2), 110–118 (2004)
7. Clemente, P., Murulo, F., Lece, L., Bifulco, A.: Experimental modal analysis of the Garigliano cable-stayed bridge. Soil Dyn. Earthq. Eng. **17**, 485–493 (1998)
8. McDougall, D., Green, M., Shillinglaw, S.: Fatigue damage of steel bridges due to dynamic vehicle loads. J. Bridg. Eng. **11**(3), 320–328 (2006)
9. Wang, T., Liu, Ch., Huang, D., Shahawy, M.: Truck loading and fatigue damage analysis for girder bridges on weigh-in-motion data. J. Bridg. Eng. **10**(1), 12–20 (2005)
10. Kim, H., Adeli, H.: Wavelet-hybrid feedback linear mean squared algorithm for robust control of cable-stayed bridges. J. Bridg. Eng. **10**(2), 116–123 (2005)
11. Chang, K., Mo, Y., Chen, C., Lai, L., Chou, C.: Lessons learned from the damaged Chi–Lu cable-stayed bridge. J. Bridg. Eng. **9**(4), 343–352 (2004)
12. Das, A., Dutta, A., Talukdar, S.: Efficient dynamic analysis of cable-stayed bridges under vehicular movement using space and time adaptivity. Finite Elem. Anal. Des. **40**, 407–424 (2004)
13. Xu, Y., Zhang, N., Xia, H.: Vibration of coupled train and cable-stayed bridge systems in cross winds. Eng. Struct. **26**, 1389–1406 (2004)
14. Carrion, F., Doyle, J., Lozano, A.: Structural health monitoring and damage detection using a sub-domain inverse method. Smart Mater. Struct. **12**(5), 776–784 (2003)
15. Xu, B., Wu, Z., Yokoyama, K.: Neural networks for decentralized control of cable-stayed bridge. J. Bridg. Eng. **8**(4), 229–236 (2003)
16. Wong, K., Chan, K., Man, K.: Monitoring of wind load and response of cable-supported bridges in Hong Kong. In: Health Monitoring and Management of Civil Infrastructure Systems. Proceedings of SPIE, vol. 4337, pp. 292–303 (2001)
17. Phelan, R., Sarker, P., Mehta, K.: Full scale measurements to investigate rain-wind induced cable-stay vibration and its mitigation. J. Bridg. Eng. **11**(3), 293–304 (2006)
18. Berglund, E., Schultz, A.: Girder differential deflection and distortion-induced fatigue in skewed steel bridges. J. Bridg. Eng. **11**(2), 169–177 (2006)
19. Au, F., Cheng, Y., Cheung, Y., Zheng, D.: On the determination of natural frequencies and mode shapes of cable-stayed bridges. Appl. Math. Model. **25**, 1099–1115 (2001)
20. Ni, Y., Fan, K., Zheng, G., Chan, T., Ko, J.: Automatic Modal identification of cable-supported bridges instrumented with a long-term monitoring system. In: Smart Structures and Materials. Proceedings of SPIE, vol. 5057, pp. 329–339 (2003)
21. Zhang, Y., Zhang, Z., Xu, X., Hua, H.: Modal parameter identification using response data only. J. Sound Vib. **282**, 367–380 (2005)
22. Zhengsheng, L., Swanson, A., Helmicki, A., Hunt, V.: Modal contribution coefficients in bridge condition evaluation. J. Bridg. Eng. **10**(2), 169–178 (2005)
23. Ren, W., Peng, X., Lin, Y.: Experimental and analytical studies on dynamic characteristics of a large span cable-stayed bridge. Eng. Struct. **27**, 535–548 (2005)
24. Lui, Y., Gordaninejad, F., Evrensel, C., Hitchcock, G.: An experimental study on fuzzy logic vibration control of bridge using fail-safe magneto-rheological fluid dampers. In: Smart Structures and Materials. Proceedings of SPIE, vol. 4330, pp. 281–288 (2001)
25. Ni, Y., Spencer, B., Ko, J.: Feasibility of active control of cable-stayed bridges: an insight into Ting Kau Bridge. In: Smart Structures and Materials. Proceedings of SPIE, vol. 4330, pp. 387–398 (2001)
26. Park, K., Koh, H., Ok, S., Seo, C.: Fuzzy supervisory control of earthquake-excited cable-stayed bridges. Eng. Struct. **27**, 1086–1100 (2005)
27. Carrión, F.: Experimental assessment for the nonlinear behavior of the cables in a cable stayed bridge (2007, in preparation)
28. Xu, L., Yu, Z.: Vibration of Inclined sag cables with oil dampers in cable-stayed bridges. J. Bridg. Eng. **3**(4), 194–203 (1998)
29. Irvine, M.: Cable Structures, 2nd edn., pp. 3–20. Dove, New York (1981)
30. Streeter, V., Wylie, B.: Fluid Mechanics, 7th edn., p. 223. McGraw–Hill, New York (1979)
31. Clough, R.W., Penzien, J.: Dynamics of Structures, 2nd edn., pp. 31–54. McGraw–Hill, Singapore (1993)
32. McConnell, K.G.: Vibration Testing, 1st edn. Wiley–Interscience, New York (1995)